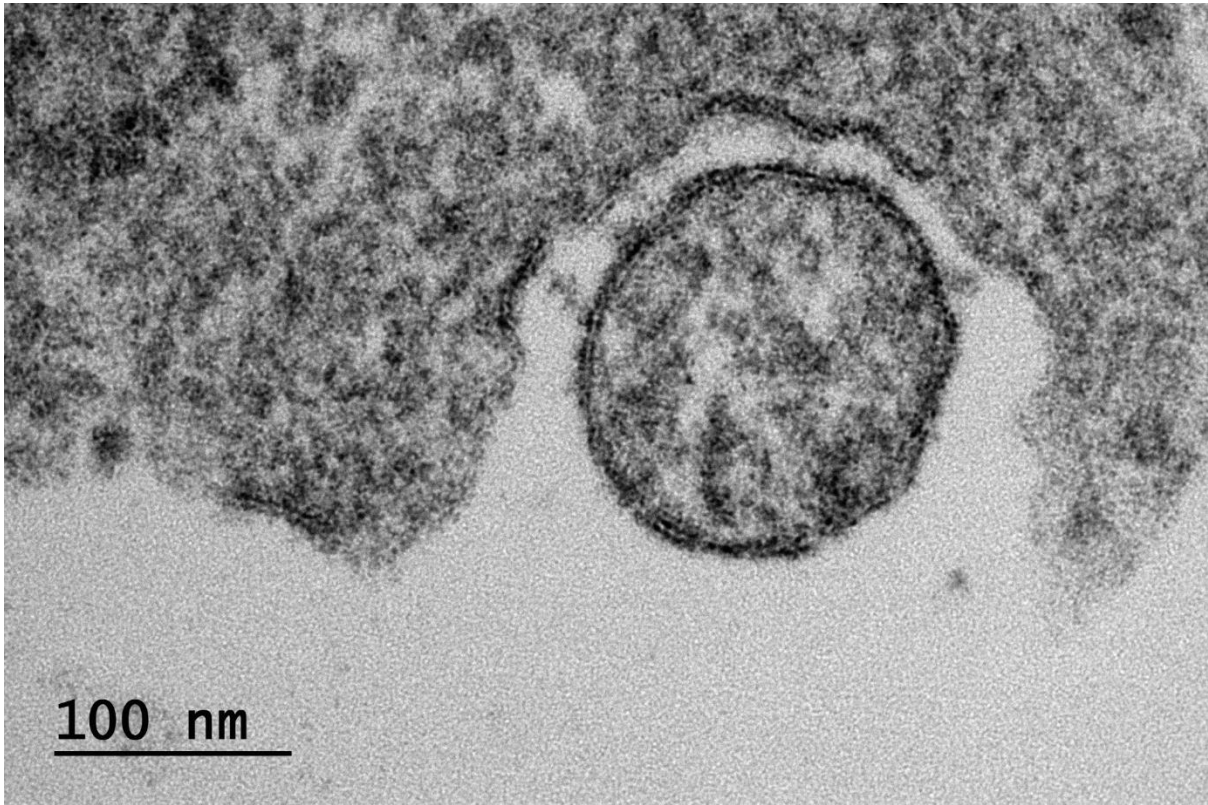**Supplementary figures**

Figure S1. Internalization of a SARS-CoV-2Wu:(E,S,M) observed via thin-section electron microscopy of murine lung epithelial (*MLE*) cells. A VLP can be seen bound to the plasma membrane via the SARS-CoV-2 S protein.
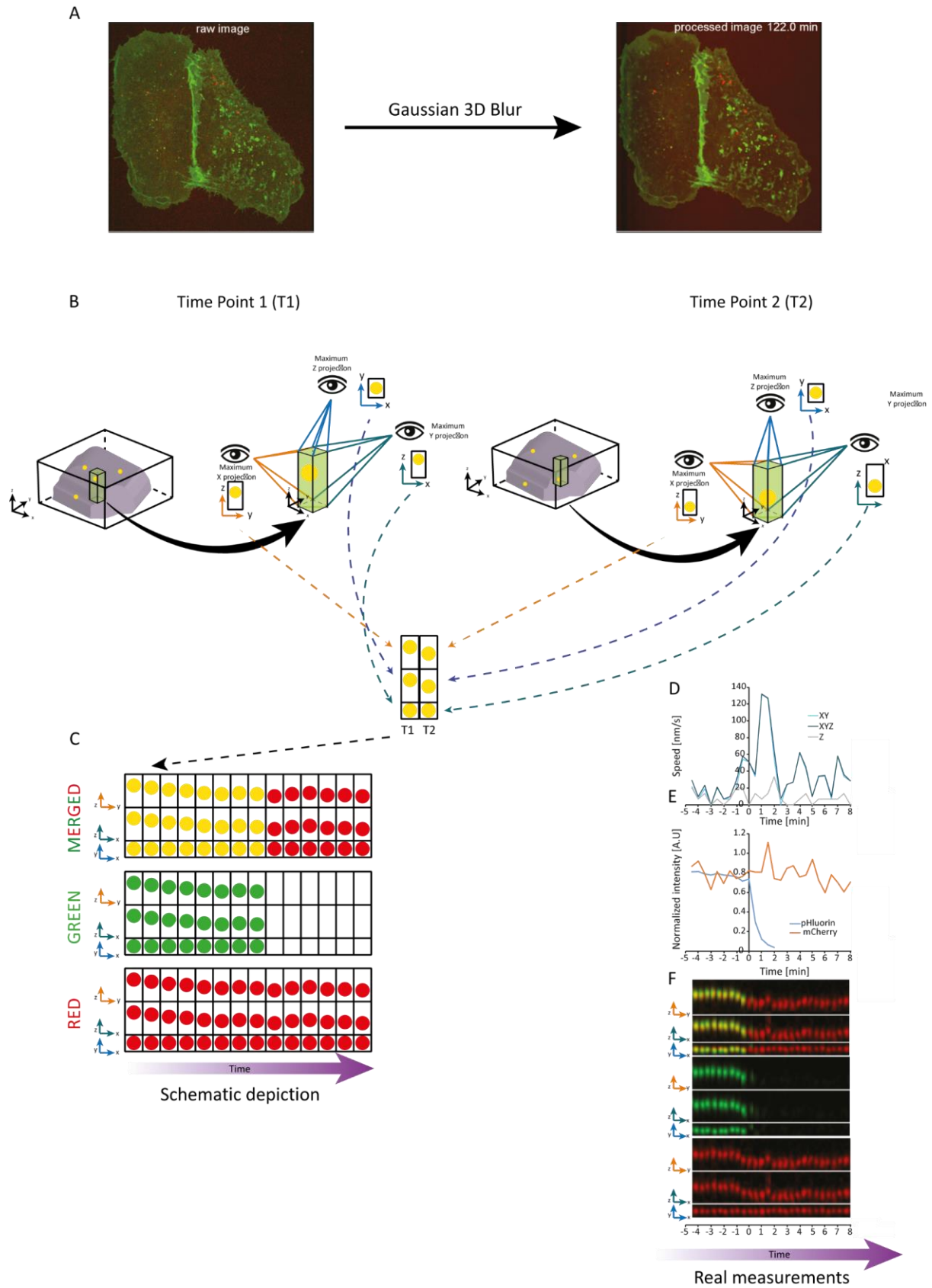
Figure S2. Schematic representation of the SPARTACUSS pipeline for measurement and analysis of VLP internalization dynamics.

A. Gaussian 3D blurring of the raw image to make the VLPs more distinct.

B. A schematic 3D representation of a cell (gray volume inside black cube) imaged over two consecutive time points. Single VLPs are presented as yellow dots (merged signal mCherry and pHluorin). A volume (green parallelepiped) around a VLP of interest is chosen, and maximum intensity projections along each axis (eye viewpoints) are extracted and combined vertically. The combined projections from the two time points are then horizontally compiled in a sequence to generate a kymograph.

C. Schematic kymographs of a single VLP tracked over time, acquired in two imaging channels: green (middle), red (bottom), and merged (top). If the signal in the green channel disappears, the VLP in the merged kymograph changes from yellow to red. For each channel, the different axis projections are presented (ZY - top, ZX- middle, YX - bottom) as kymographs.

D. Measurements of the speed of a single VLP using the pipeline described above. Each point in the top graph represents the speed of the particle over time extracted from two consecutive images in 1D-vertically (Z), 2D (XY), and 3D (XYZ)

E. Measurement of the intensity of a single VLP for each time point in the two different channels.

F. Kymograph of a single SARS-CoV-2 VLP acquired in two channels (Green-M-pHluorin, Red-M-mCherry), presented as described in (B).
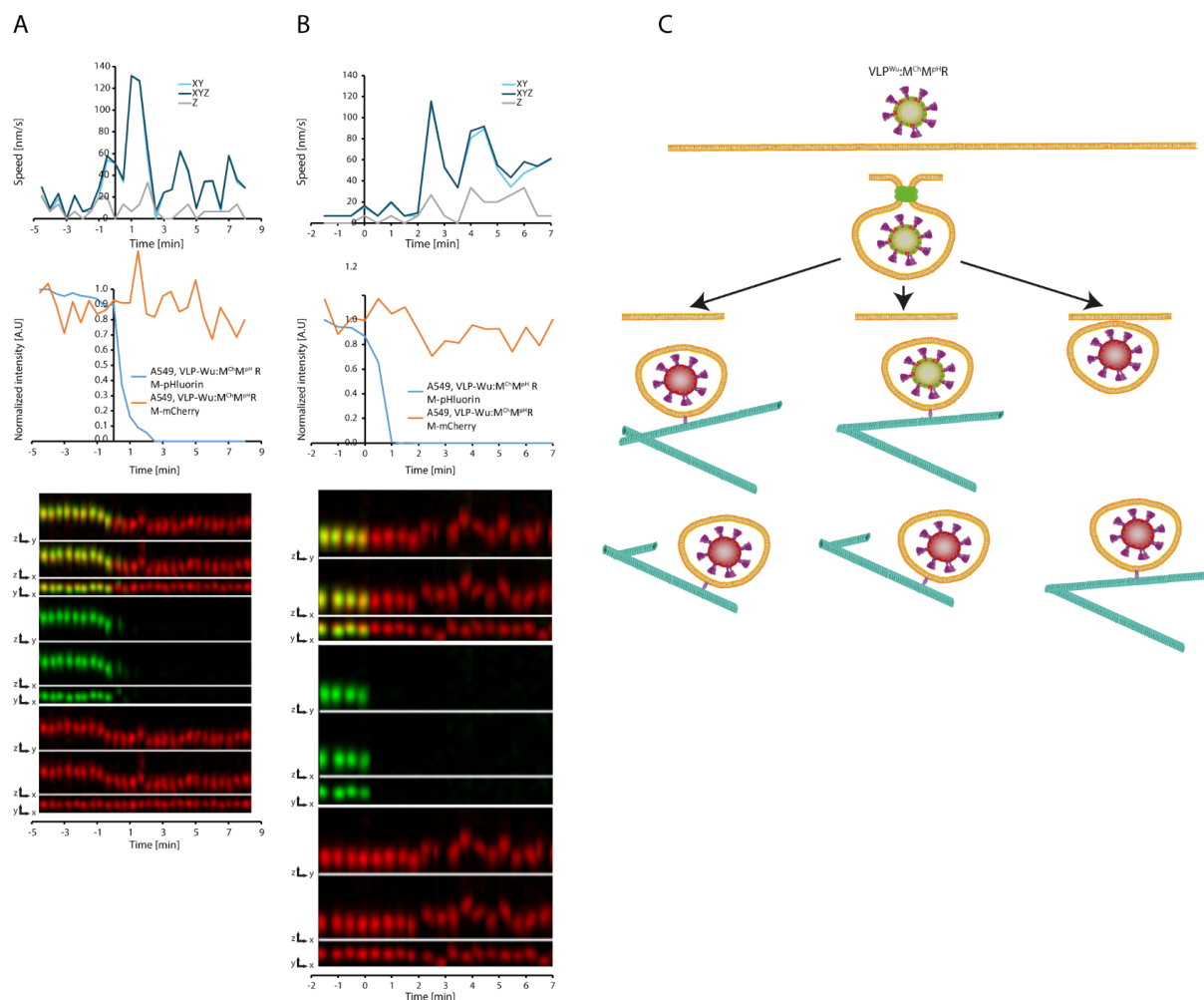
Figure S3. Example of single VLP^{Wu}:M^{Ch}M^{pH}R entries into A549 cells.

A. Representative VLP speed and intensity graphs (top) and kymographs (merged, M-mCherry, and M-pHluorin) in all dimensions (bottom) for a single VLP undergoing internalization, where the speed of the particle increases before its pHluorin intensity starts to decrease.

B. Same as (A), but for a VLP the speed of which increases after its pHluorin intensity starts to decrease.

C. Schematic representation of the VLP acidification and microtubule attachment (speed increase); The pH drops simultaneously with the start of active microtubule movement (Left); The pH drops below 5 after the start of active microtubule movement (Middle); The pH of the VLP drops below 5 before active microtubule movement (Right);
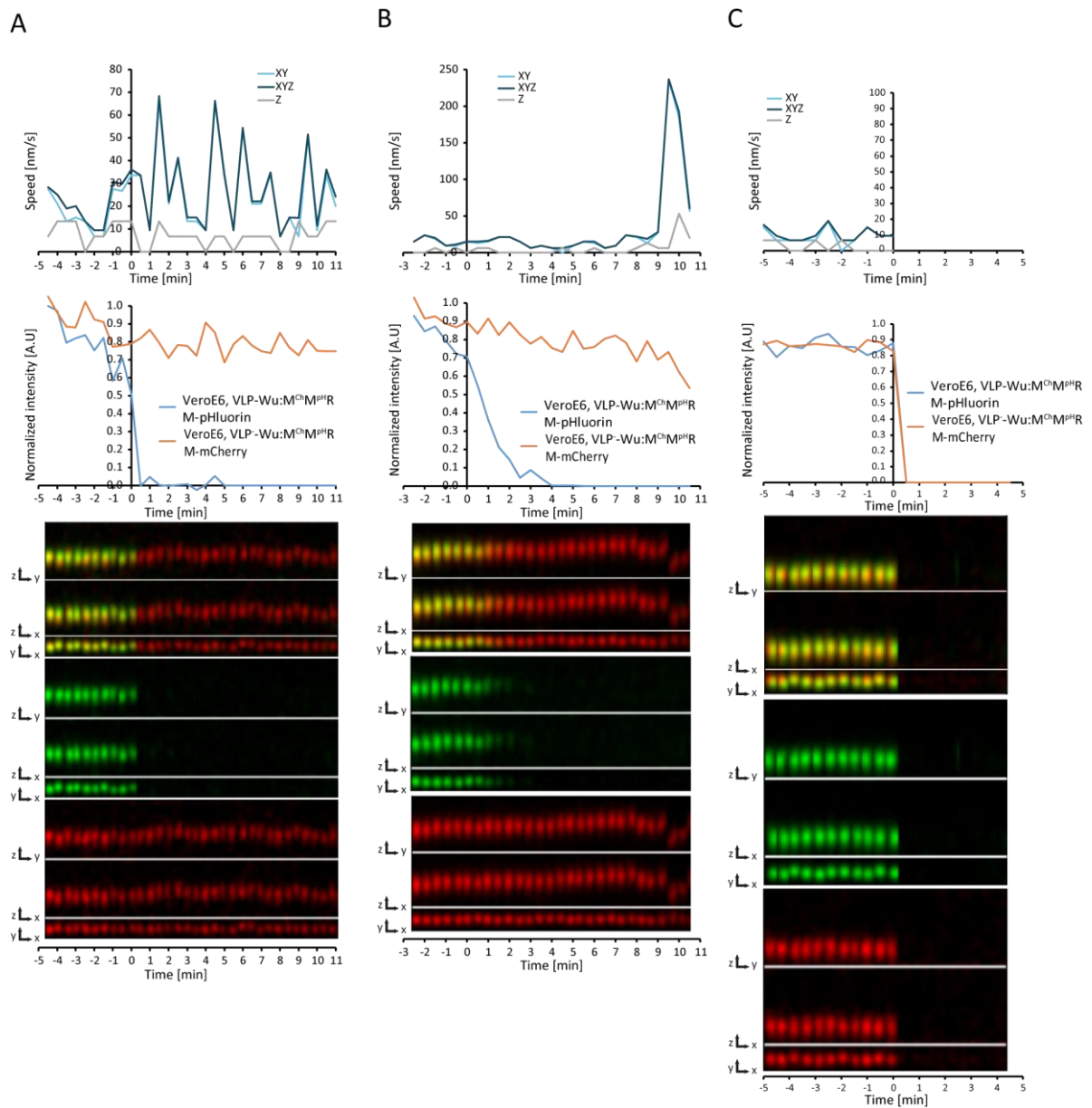
Figure S4. Example of single VLP^{Wu}:M^{Ch}M^{pH}R entries into Vero E6 cells.

A. Representative VLP speed and intensity graphs (top) and kymographs (merged, M-mCherry, and pHluorin) in all dimensions (bottom) for a single VLP undergoing internalization, where the speed of the particle increases before its pHluorin intensity starts to decrease.

B. Same as (A), but for a VLP the speed of which increases after its pHluorin intensity starts to decrease.

C. Same as (A), but for a VLP for which the signals of both fluorescent proteins disappear simultaneously.
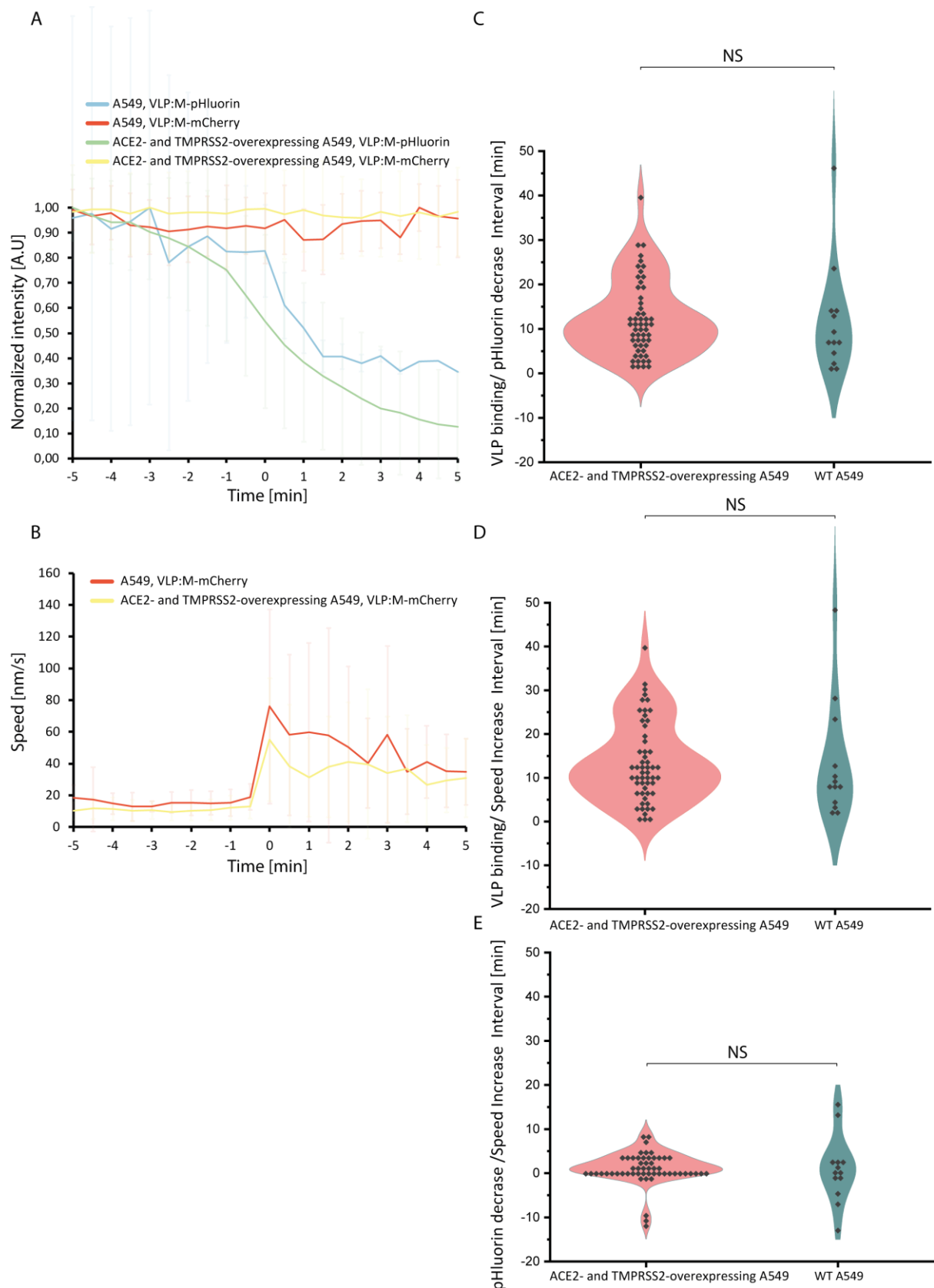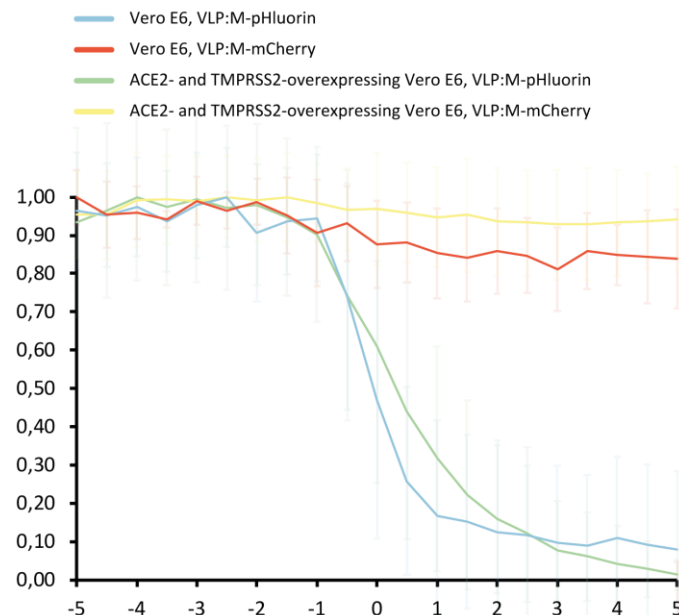
Figure S5. **Comparison of VLP^Wu: M^ChM^pHR binding, acidification, and speed increase dynamics in A549 cells with and without overexpression of ACE2 and TMPRSS2.**

A. Comparison of pHluorin intensity decrease during the internalization of VLP^Wu: M^ChM^pHR in A549 cells with and without overexpression of ACE2 and TMPRSS2. The average intensity of pHluorin is represented as a function of time where the individual
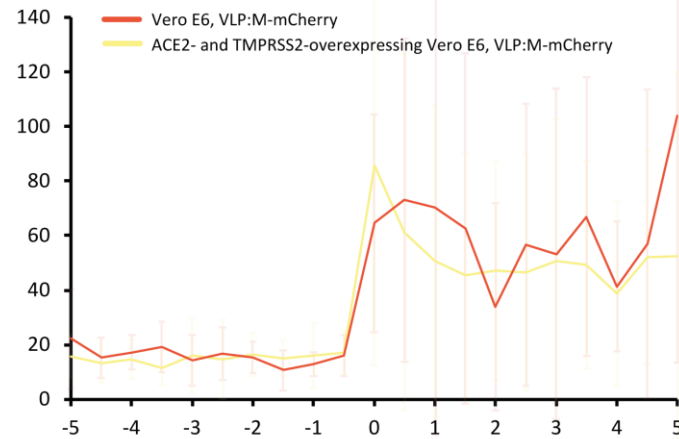
VLPs were aligned to the start of VLP pHluorin decrease (0 min). The average M-mCherry intensity is also presented. Error bars represent the standard deviation.

B. The average speed of VLP^{Wu}:M^{Ch}M^{pH}R in A549 cells with and without overexpression of ACE2 and TMPRSS2 measured based on the tracked M-mCherry signal. The average speed of VLPs was calculated after alignment of the individual VLP speeds to the start of the VLP pHluorin signal decrease (0 min). Error bars represent the standard deviation.

C. Distribution of time intervals between VLP binding and start of pHluorin intensity decrease for individual VLP^{Wu}: M^{Ch}M^{pH}R during internalization in A549 cells with and without overexpression of ACE2 and TMPRSS2. T wo-tailed Student's t-test; NS $p>0.01$; * $p<0.01$.

D. Distribution of time intervals between VLP binding and speed increase for individual VLP^{Wu}: M^{Ch}M^{pH}R, during internalization in A549 cells with and without overexpression of ACE2 and TMPRSS2. T wo-tailed Student's t-test; NS $p>0.01$; * $p<0.01$.

E. Distribution of time intervals between start of pHluorin intensity decrease and speed increase for individual VLP^{Wu}: M^{Ch}M^{pH}R, during internalization in A549 cells with and without overexpression of ACE2 and TMPRSS2. Two-tailed Student's t-test; NS $p>0.01$; * $p<0.01$.
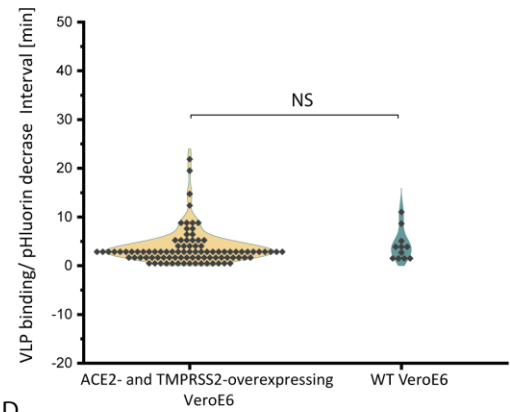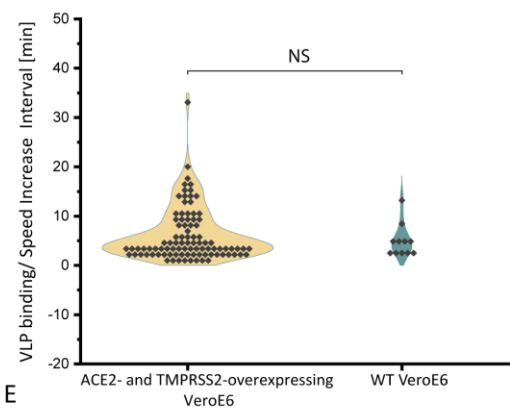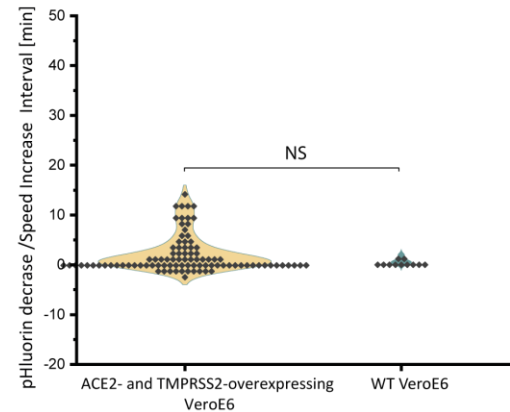
Figure S6. Comparison of VLP^{Wu}: M^{Ch}M^{pH}R binding, acidification, and speed increase dynamics in VeroE6 cells with and without overexpression of ACE2 and TMPRSS2.

A. Comparison of pHluorin intensity decrease during the internalization of VLP^{Wu}: M^{Ch}M^{pH}R in VeroE6 cells with and without overexpression of ACE2 and TMPRSS2. The average intensity of pHluorin is represented as a function of time where the individual VLPs were aligned to the start of VLP pHluorin decrease (0 min). The average M-mCherry intensity is also presented. Error bars represent the standard deviation.

B. The average speed of VLP^{Wu}:M^{Ch}M^{pH}R in VeroE6 cells with and without overexpression of ACE2 and TMPRSS2 measured based on the tracked M-mCherry signal. The average speed of VLPs was calculated after alignment of the individual VLP speeds to the start of the VLP pHluorin signal decrease (0 min). Error bars represent the standard deviation.

C. Distribution of time intervals between VLP binding and start of pHluorin intensity decrease for individual VLP^{Wu}: M^{Ch}M^{pH}R, during internalization in VeroE6 cells with and without overexpression of ACE2 and TMPRSS2. Two-tailed Student's t-test; NS $p>0.01$; * $p<0.01$.

D. Distribution of time intervals between VLP binding and speed increase for individual VLP^{Wu}: M^{Ch}M^{pH}R during internalization in VERO E6 cells with and without overexpression of ACE2 and TMPRSS2. Two-tailed Student's t-test; NS $p>0.01$; * $p<0.01$.

E. Distribution of time intervals between start of pHluorin intensity decrease and speed increase for individual VLP^{Wu}: M^{Ch}M^{pH}R during internalization in VeroE6 cells with and without overexpression of ACE2 and TMPRSS2. Two-tailed Student's t-test; NS $p>0.01$; * $p<0.01$.
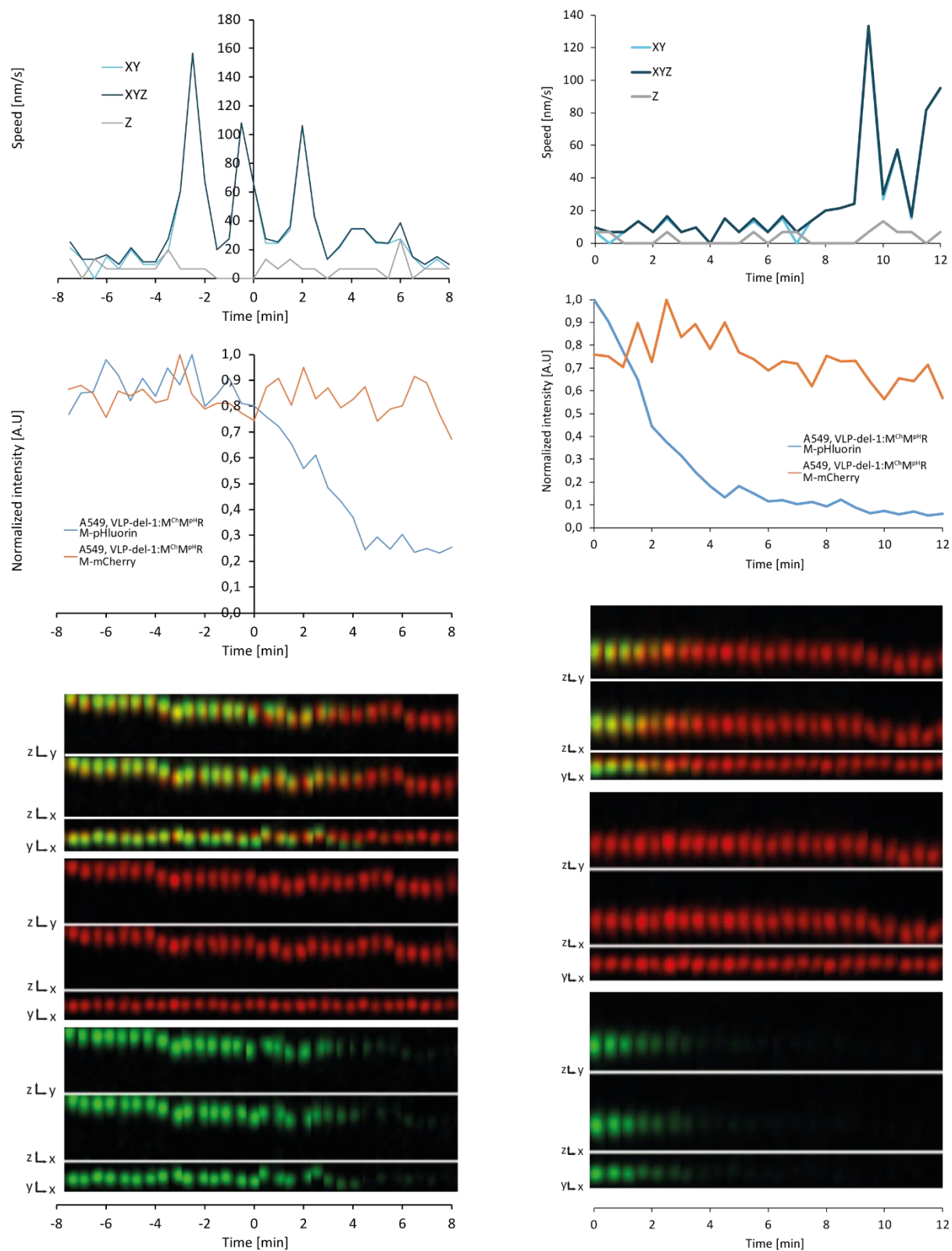
Figure S7. Example of single VLP$^{\text{del-1}}$:M$^{\text{Ch}}$M$^{\text{pH}}$R entry into A549 cells.

A. Representative VLP speed and intensity graphs (top) and kymographs (merged, M-mCherry, and pHluorin) in all dimensions (bottom) for a single VLP undergoing internalization, where the speed of the particle increases before its pHluorin intensity starts to decrease.

B. Same as (A), but for a VLP the speed of which increases after its pHluorin intensity
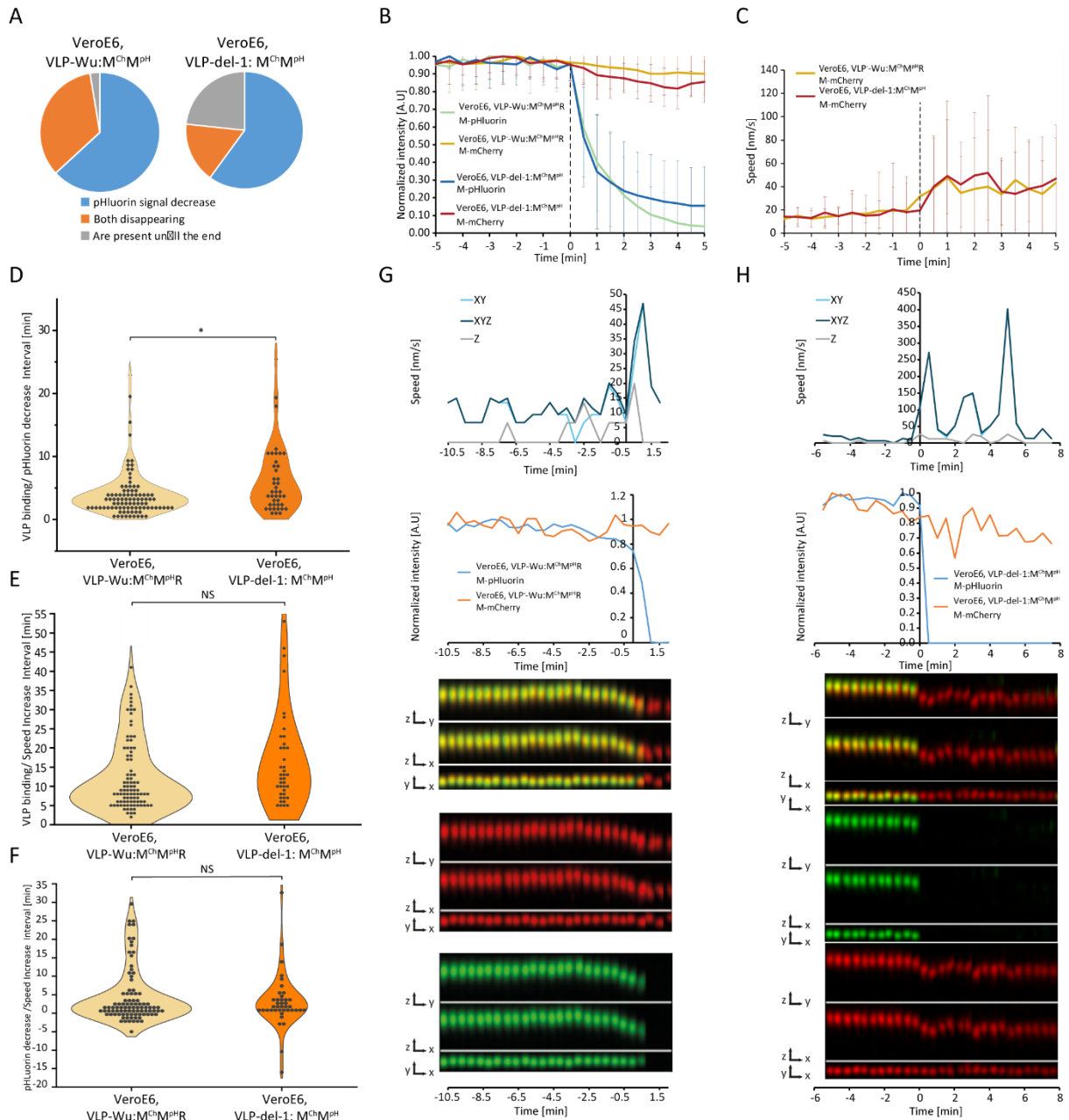
C. starts to decrease.

Figure S8. Dynamics of VLP binding and speed increase for VLP^Wu:M^ChM^pH and VLP^del-1:M^ChM^pH during internalization in VeroE6 cells.

A. Percentage of VLPs in which only the M-pHluorin intensity decreases (Blue), M-pHluorin and M-mCherry intensities decrease simultaneously (Orange), or neither decreases (Gray).

B. Comparison of pHluorin intensity decrease during the internalization of VLP^{Wu}: $M^{Ch}M^{pH}R$ and VLP^{del-1}: $M^{Ch}M^{pH}R$ in VeroE6 cells. The average intensity of pHluorin is represented as a function of time where the individual VLPs were aligned to the start of VLP pHluorin decrease (0 min). The average M-mCherry intensity is also presented. Error bars represent the standard deviation. For VeroE6-VLP^{Wu}:$M^{Ch}M^{pH}R$ n=93, for VeroE6-VLP^{del-1}:$M^{Ch}M^{pH}$ n=41.

C. Comparison of the dynamics of speed increase of VLP^{Wu}:$M^{Ch}M^{pH}$ and VLP^{del-1}:$M^{Ch}M^{pH}$ internalization in Vero E6 cells. The average speed of VLPs is presented as a function of time where the individual VLPs were aligned to the start of M-pHluorin decrease (0 min). Error bars represent the standard deviation. For VeroE6-VLP^{Wu}:$M^{Ch}M^{pH}$ n=93, for VeroE6-VLP^{del-1}:$M^{Ch}M^{pH}$ n=41.

D. Distribution of time intervals between VLP^{Wu}:$M^{Ch}M^{pH}$ and VLP^{del-1}:$M^{Ch}M^{pH}$ binding and start of the decrease in pHluorin intensity during internalization in VeroE6 cells. Two-tailed Student's t-test; NS p>0.01; * p<0.01. For VeroE6-VLP^{Wu}:$M^{Ch}M^{pH}$ n=93, for VeroE6-VLP^{del-1}:$M^{Ch}M^{pH}$ n=41.

E. Distribution of time intervals between VLP^{Wu}:$M^{Ch}M^{pH}$ and VLP^{del-1}:$M^{Ch}M^{pH}$ binding and start of VLP speed increase in VeroE6 cells. Two-tailed Student's t-test; NS p>0.01; * p<0.01. For VeroE6-VLP^{Wu}:$M^{Ch}M^{pH}$ n=93, for VeroE6-VLP^{del-1}:$M^{Ch}M^{pH}$ n=41.

F. Distribution of time intervals between VLP^{Wu}:$M^{Ch}M^{pH}$ and VLP^{del-1}:$M^{Ch}M^{pH}$ pHluorin intensity decrease and start of VLP speed increase in VeroE6 cells. Two-tailed Student's t-test; NS p>0.01; * p<0.01. For VeroE6-VLP^{Wu}:$M^{Ch}M^{pH}$ n=93, for VeroE6-VLP^{del-1}:$M^{Ch}M^{pH}$ n=41.

G. Representative VLP speed and intensity graphs (top) and kymographs (merged, M-mCherry, and pHluorin) in all dimensions (bottom) for a single VLP^{Wu}:$M^{Ch}M^{pH}$ undergoing internalization in a VeroE6 cell.
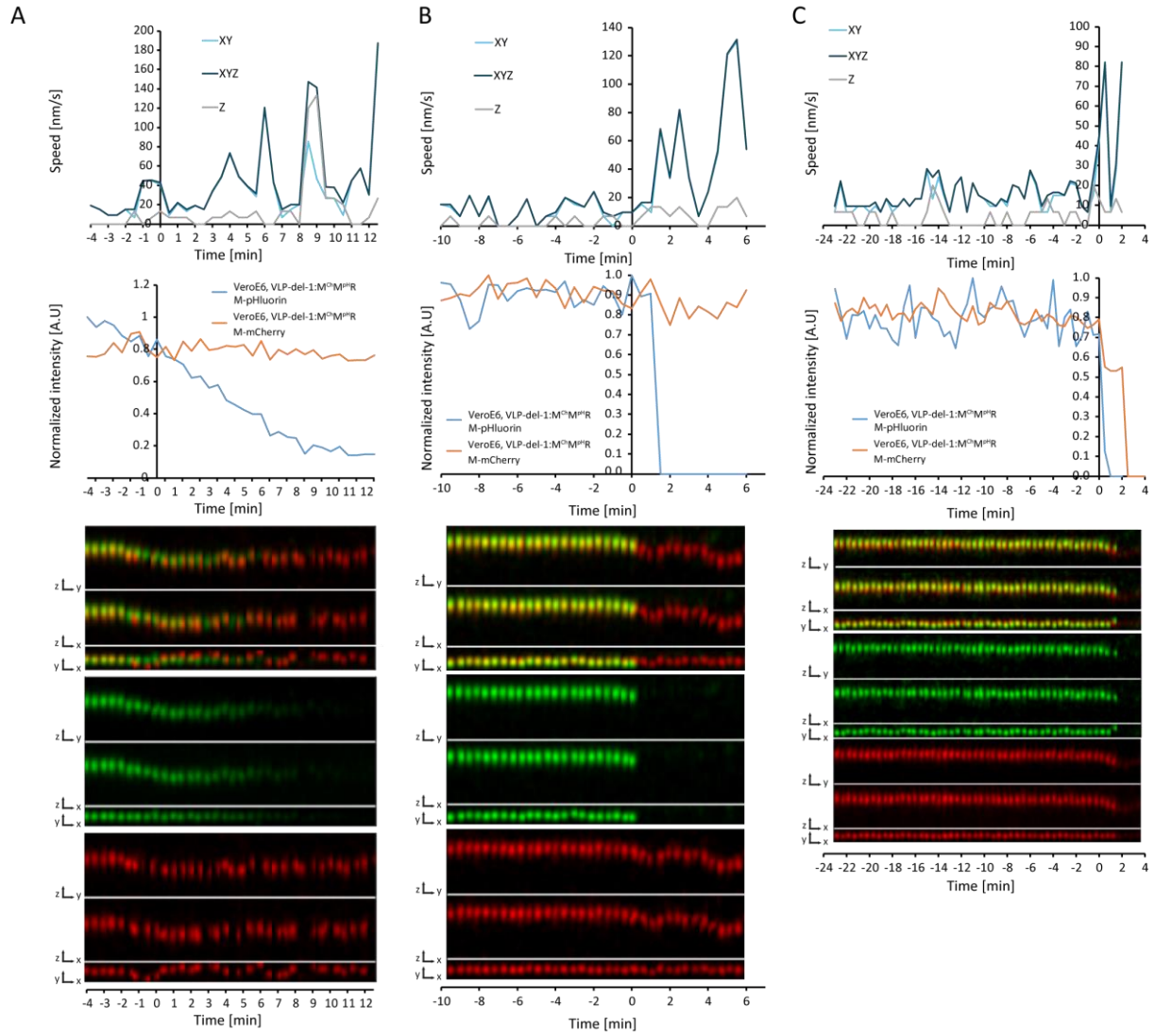
H. Same as (G) for VLP^{del-1}:$M^{Ch}M^{pH}$.

Figure S9. Examples of a single VLP^{del-1}:M^{Ch}M^{pH} entry into Vero E6 cells.

A. Representative VLP speed and intensity graphs (top) and kymographs (merged, M-mCherry, and pHluorin) in all dimensions (bottom) for a single VLP undergoing internalization, where the speed of the particle increases before its pHluorin intensity starts to decrease.

B. Same as (A), but for a VLP the speed of which increases after its pHluorin intensity starts to decrease.

C. Same as (A), but for a VLP for which the signals of both fluorescent proteins disappear simultaneously.
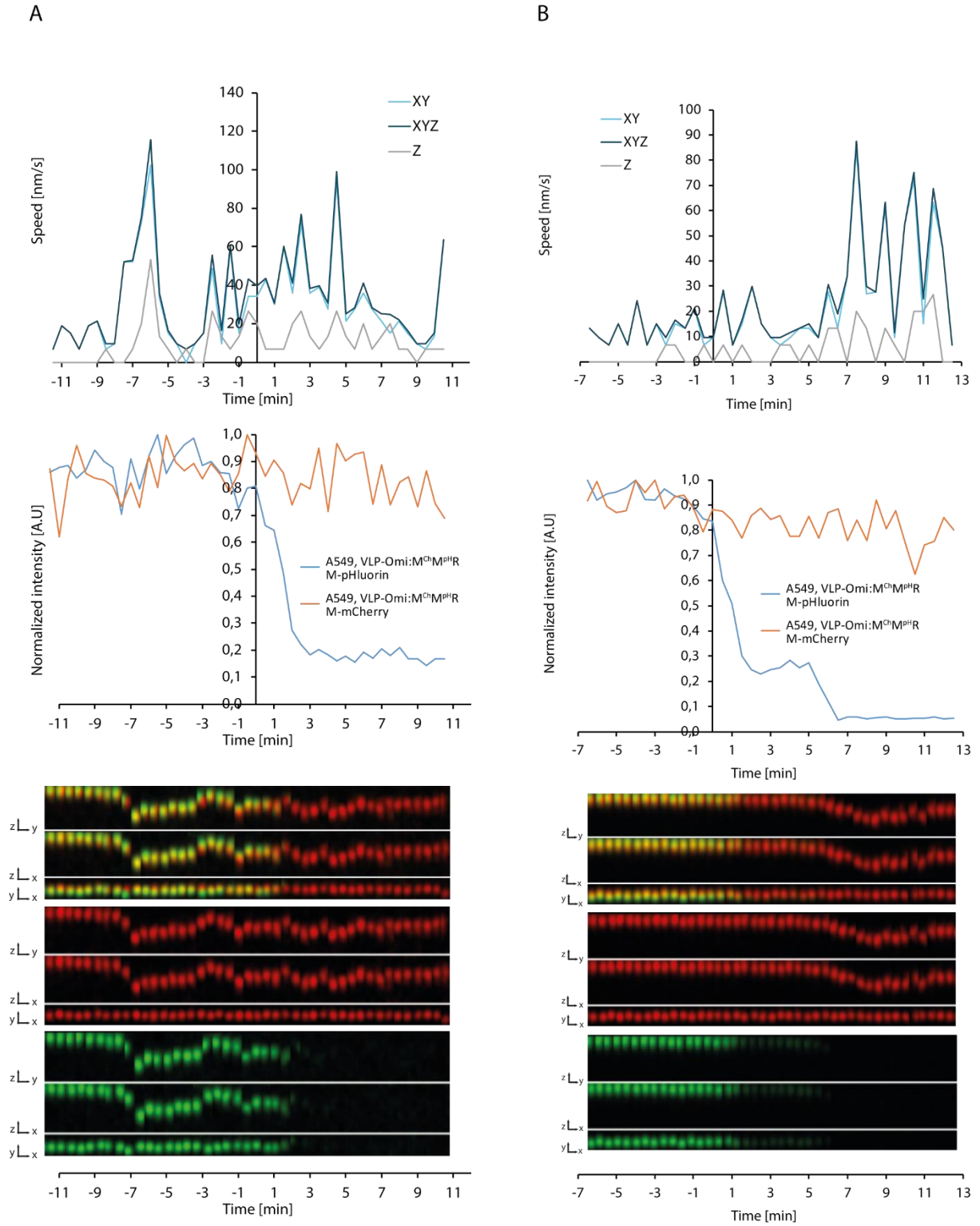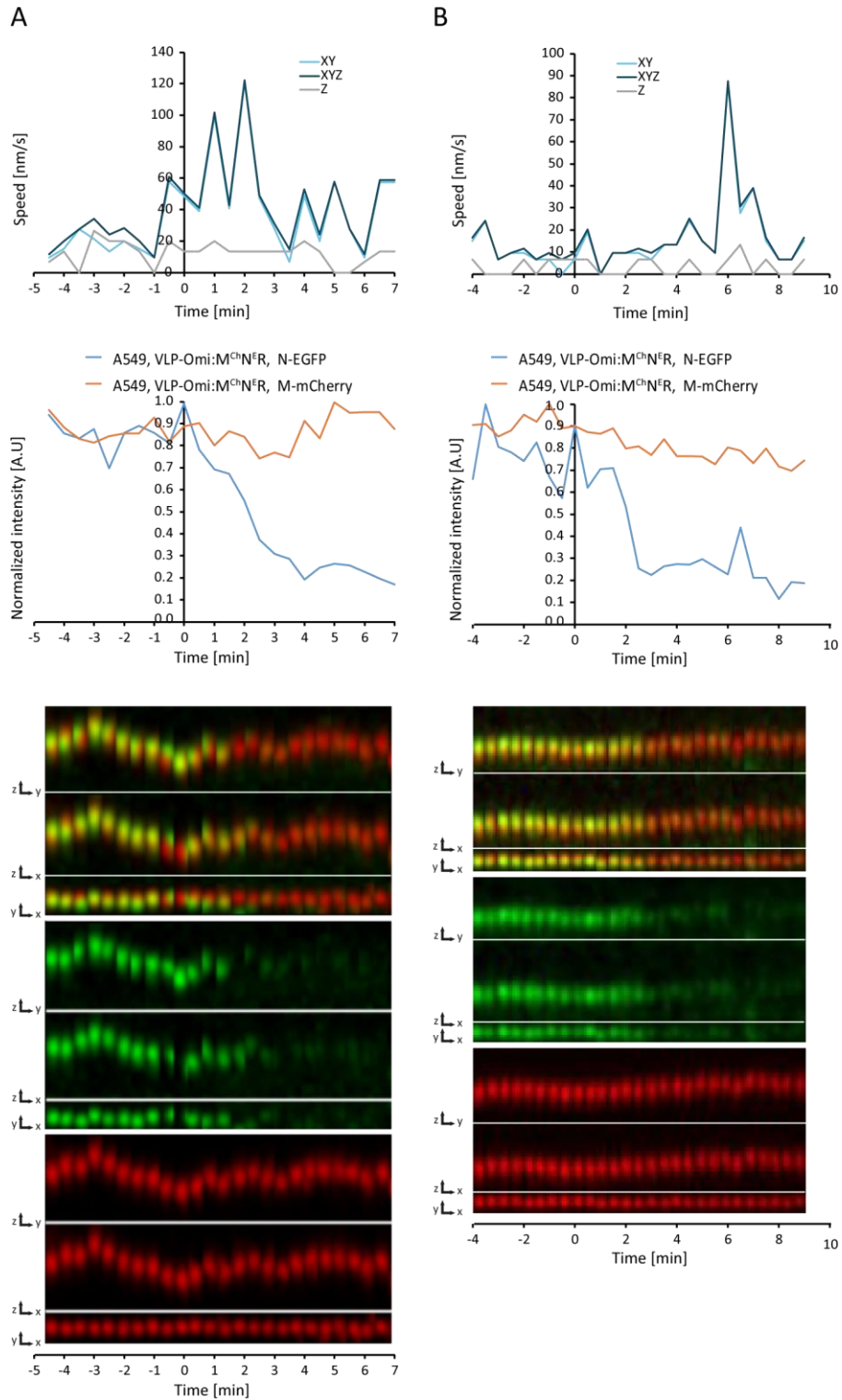
Figure S10. Examples of single VLP^{Omi}:M^{Ch}M^{pH}R entries into A549 cells.

A. Representative VLP speed and intensity graphs (top) and kymographs (merged, M-mCherry, and pHluorin) in all dimensions (bottom) for a single VLP undergoing

internalization, where the speed of the particle increases before its pHluorin intensity starts to decrease.

B. Same as (A), but for a VLP the speed of which increases after its pHluorin intensity starts to decrease.

Figure S11. Examples of single VLP^{Omi}:M^{Ch}N^{E}R entries into A549 cells.

A. Representative VLP speed and intensity graphs (top) and kymographs (merged, M-mCherry, and N-EGFP) in all dimensions (bottom) for a single VLP undergoing internalization, where the speed of the particle increases before its pHluorin intensity starts to decrease.

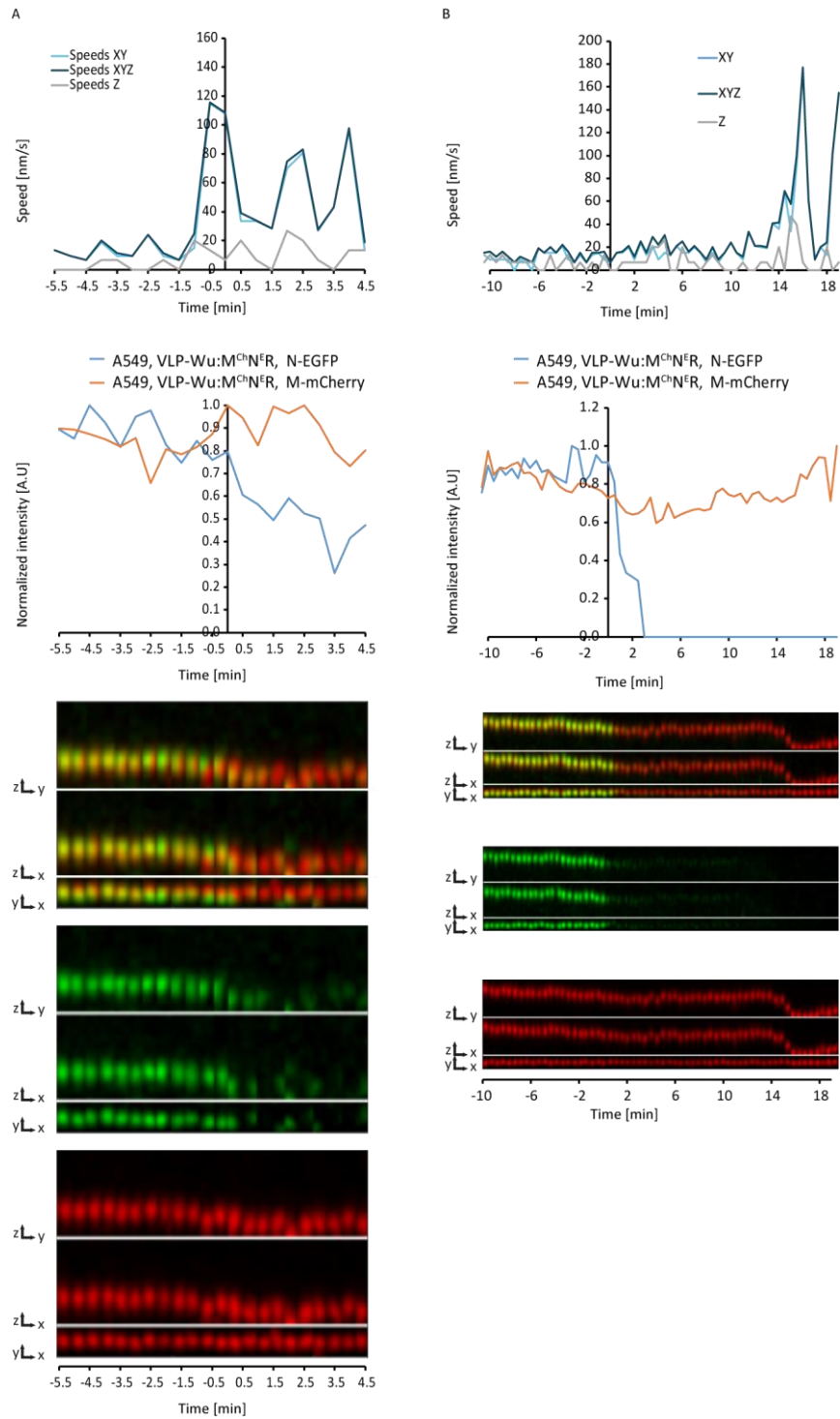B. Same as (A), but for a VLP the speed of which increases after its pHluorin intensity starts to decrease.

Figure S12. Examples of single VLP^{Wu}:M^{Ch}N^ER entries into A549 cells.

A. Representative VLP speed and intensity graphs (top) and kymographs (merged, M-mCherry, and N-EGFP) in all dimensions (bottom) for a single VLP undergoing internalization, where the speed of the particle increases before its pHluorin intensity starts to decrease.

B. Same as (A), but for a VLP the speed of which increases after its pHluorin intensity starts to decrease.